The Enzymatic Properties of *Octopus vulgaris* Hemocyanin: *o*-Diphenol Oxidase Activity†

Benedetto Salvato,*,‡,§ Meri Santamaria,‡ Mariano Beltramini,‡,§ Gloria Alzuet,|| and Luigi Casella||

Department of Biology and CNR Center for the Biochemistry and Physiology of Metalloproteins, University of Padova, Via Ugo Bassi, 58/B, I-35131 Padova, Italy, and Department of General Chemistry, University of Pavia, Via Taramelli 12, I-27100 Pavia, Italy

Received April 20, 1998; Revised Manuscript Received June 29, 1998

ABSTRACT: Hemocyanin and tyrosinase are dinuclear copper proteins capable of reversibly binding dioxygen. Despite the great similarity of structure and properties of their active site, the two proteins perform different biological functions (oxygen transport/storage versus monooxygenase and oxidase activity). In this paper, we show that *Octopus vulgaris* hemocyanin exhibits a tyrosinase-like activity; namely, it is capable of utilizing dioxygen for the oxidation of *o*-diphenol to quinone. The reaction is specific for this isomer of diphenol, the meta and para isomers being unreactive, and is strongly controlled by steric factors. Dioxygen represents a cosubstrate of the reaction, and it is involved in the catalytic turnover by binding to the dinuclear copper site of the protein to form, under steady-state conditions, oxy-Hc, which is the active species. The generation of semiquinone radicals, detected by EPR and by their reaction with *N*,*N*,*N*′,*N*′-tetramethyl-1,4-phenylenediamine, strongly supports a reaction mechanism in which such radicals represent the reaction products of one-electron oxidation of the substrate, quinone being generated by dismutation of semiquinones. Met-Hc is regenerated by the substrate to the deoxy form. To close the catalytic cycle, the proposed reaction mechanism also involves the participation of two transient protein forms with the total oxidation state of the active site (V and IV) intermediate between that of oxy-Hcy, $[Cu^{II}O_2^{2-}Cu^{II}]^{VI}$, and deoxy-Hc, $[Cu^{I}Cu^{I}]^{II}$. A mathematical model has been elaborated to describe the reaction kinetics. The differences in reaction mechanisms between hemocyanin and tyrosinase are discussed in terms of accessibility to exogenous molecules of their active sites.

Hemocyanins (Hcs)[1] are high molecular weight proteins in the hemolymph of several molluscan and arthropodan species where they play a dioxygen transport and/or storage function, based on their capability to bind reversibly molecular oxygen in an active site containing a pair of copper ions (dinuclear-coupled copper site) (*1*).

The first X-ray crystallography model at 0.32 nm resolution has been proposed for the deoxygenated form of the Hc isolated from the arthropod *Panulirus interruptus* (*2*). Each metal ion is bound to three histidine residues, two of which are located at 0.19 nm bonding distance with the third one at 0.27 nm. The four nitrogens at shorter distance together with the two copper ions are almost coplanar, whereas the other two lie on the opposite sides of this plane. The copper−copper distance is about 0.36 nm. The active site is deeply buried in the protein matrix and surrounded by hydrophobic residues. The model for subunit II of *Limulus polyphemus* (Arthropoda) deoxy-Hc (*3*), also derived by X-ray analysis, involves an approximate trigonal planar coordination for copper with a metal−metal distance of 0.46 nm.

The binding of dioxygen occurs via an internal reversible electron transfer involving the active site metals and the dioxygen molecule. Thus, in the deoxy form, the metal is present in the Cu(I) state while in the oxy form the active site contains a $[Cu^{II}O_2^{2-}Cu^{II}]$ complex. In the oxy-Hc crystal structure from *Limulus*, each Cu(II) ion is five-coordinate in a square pyramidal geometry, the equatorial plane being defined by two histidine nitrogens and the bound peroxide, which forms a $\mu-\eta^2:\eta^2$ peroxo bridge between the two Cu(II) ions. The five-coordination is completed by the third axial histidine of each copper. The metal−metal distance is shortened to 0.36 nm (*4*, *5*), a value in very good agreement with EXAFS[1] data (*6*).

The Cu(II)−peroxide adduct is responsible for the peculiar spectroscopic properties of the oxygenated form of the protein: an intense absorption band at approximately 340 nm ($\epsilon \approx 20\,000$ M^{-1} cm^{-1}) and a broader feature with an apparent maximum around 570 nm ($\epsilon \approx 1000$ M^{-1} cm^{-1}) characterize the near-ultraviolet−visible electronic spectrum of oxy-Hc from both *phyla*. Both bands arise from peroxide-

† This work was supported by grants from MURST (ex-40% and ex-60% grants to M.B. and B.S.), CNR (to M.B. and B.S.), and European Community (Contracts ERBCHRXCT920014 and ERBCHBICT930312 to L.C. and G.A.).

* To whom correspondence should be addressed at the Department of Biology, University of Padova, Via Ugo Bassi, 58/B, I-35131 Padova, Italy.

‡ Department of Biology, University of Padova.

§ CNR Center for the Biochemistry and Physiology of Metalloproteins, University of Padova.

|| Department of General Chemistry, University of Pavia.

[1] Abbreviations: Hcs, hemocyanins; EXAFS, extended X-ray absorption fine structure; Ty, tyrosinase; EPR, electron paramagnetic resonance; HPLC, high-pressure liquid chromatography; THB, trihydroxybenzene; CD, circular dichroism.

S0006-2960(98)00879-4 CCC: $15.00
Published on Web 09/17/1998

to-Cu(II) charge-transfer transitions, the Cu(II) d−d transitions contributing to the red-edge of the lowest energy bands envelope (*1, 7*). The almost coincidence of these spectroscopic properties points to very similar active site structures in the case of molluscan and arthropod species. The results of a recent X-ray crystallography study on a functional unit of *Octopus dofleini* show that the active site of this Hc can be superimposed to that of *Limulus* with remarkable fidelity, although the overall tertiary folds of the two proteins are rather different (*8*). Furthermore, significant differences exist also as far as the sugar content and the copper-to-protein stoichiometry are concerned (*1*).

The structural and spectroscopic properties of the Hc active site were shown to be remarkably similar to those exhibited by the tyrosinase (Ty)[1] active site (*7*). Thus, in both proteins each metal ion is bound by imidazole ligands to yield a dinuclear site having approximately the same metal−metal distance (*5, 9, 10*). Like deoxy-Hc, deoxy-Ty binds reversibly molecular dioxygen at the dicuprous site to yield the active form of the enzyme, oxy-Ty, containing a dicupric−peroxide adduct (*7, 10*). Despite the great similarity of the active sites, the two proteins perform quite different biological functions: the former is a dioxygen carrier whereas the latter utilizes molecular oxygen for the *o*-hydroxylation of monophenols (monophenolase activity) and for the oxidation of *o*-diphenols to *o*-quinones (diphenolase activity). On the basis of kinetic, equilibrium, and spectroscopic studies, it has been proposed that the enzymatic activity of Ty is founded on its capability to coordinate phenolic substrates at the copper site. The transient adduct is suited either to chemical attack at the *o*-position (monophenolase activity) and/or to electron transfer involving the metal (catecholase activity) (*10, 11*).

Comparative studies on the interaction of Hc and Ty with exogenous molecules showed that the active site of both proteins reacts in the same way with respect to exogenous species. Thus, beside molecular oxygen, deoxy-Ty and deoxy-Hc reversibly bind carbon monoxide with concomitant development of a typical red-shifted luminescence (*12, 13*). The site can be chemically modified to yield half-met derivatives whose dinuclear cuprous−cupric sites display essentially the same EPR[1] spectrum (*7*). Cyanide reacts with the copper active site of both proteins competitively with respect to dioxygen but also is capable of displacing the two metal ions from the protein. In all different experimental approaches, however, the reactions on the dinuclear site occur at a much higher rate with Ty than with Hcs (*14*). Within Hcs, the proteins from molluscs are more reactive toward exogenous ligands as compared to arthropod Hcs (*7, 14, 15*). These results convincingly showed that the Ty active site is much more accessible to exogenous molecules.

Monophenolase and diphenolase activities have been reported also for some Hcs (*16, 17*). These activities, however, occur with much lower efficiency as compared to Ty, although it can be expected that they are related to some common peculiar properties of their active sites and molecular organization.

These considerations prompted us to study the interaction of *o*-diphenols with the Hc from the mollusc *Octopus vulgaris* in order to obtain further information on the specific properties of the active site which are relevant for the appearance of catalytic activity and on the modulation exerted by the protein matrix on the active site reactivity. A reaction mechanism based on oxy-Hc as active species and on substrate radical formation as a result of substrate interaction is proposed.

MATERIALS AND METHODS

Octopus vulgaris Hc was isolated as described elsewhere (*18*) from the hemolymph collected from living animals at the Zoological Station of Napoli (Napoli, Italy). The Hc from the crab *Carcinus aestuarii* was prepared from the hemolymph obtained by injection into the dorsal lacuna of living animals collected in the lagoon of Venice (*19*). The protein was stored at −20 °C in the presence of 18% (w/v) sucrose. Before use, Hc was exhaustively dialyzed against 20 mM phosphate buffer containing 10 mM EDTA and 5 mM hydroxylamine hydrochloride at pH 7.5. The protein was then dialyzed against 20 mM phosphate buffer. Hc concentration was determined spectrophotometrically using the coefficients $\epsilon = 1.43$ mL mg^{-1} cm^{-1} (for *Octopus* Hc) and 1.24 mL mg^{-1} cm^{-1} (for *Carcinus* Hc). The concentration was expressed on a molar basis using the values $M_r =$ 50K and $M_r =$ 75K relative to the species containing one active site in the case of *Octopus* and *Carcinus* Hc, respectively. The degree of oxygenation was evaluated from the absorbance ratio A_{340}/A_{278}, the values 0.25 and 0.21 corresponding to 100% oxy-Hc at pH 8.0 in the case of *Octopus* and *Carcinus* species, respectively (*18, 19*). *Octopus* semi-met- and met-Hc has been prepared according to (*20, 21*). Absorption spectra were recorded on a Perkin-Elmer Lambda 5 or on a Hewlett-Packard 8452A diode array spectrophotometer. Reagents were of the best grade commercially available and were used without further purification except *o*-diphenols and benzoic acid. The *o*-diphenols were purified by double-vacuum sublimation, and the white cristalline powder was stored at −20 °C. Benzoic acid was twice-recrystallized from water.

Kinetic Measurements. The protein (0−3.0 mg mL^{-1}), dissolved in 20 mM phosphate buffer, pH 6.0, was carefully equilibrated in air at 20 °C. The reaction was initiated by adding an aliquot of a substrate stock solution to yield the final desired concentration (0−15 mM). Quinone formation was followed by continuous recording the absorbance at 400 nm. Quinone concentration was calculated using the molar extinction coefficient $\epsilon = 1417$ M^{-1} cm^{-1} at 400 nm. The absorbance was corrected for the contribution due to the spontaneous oxidation of the substrate. This, however, occurs at a rate low enough to account for no more than 5% as compared to Hc-catalyzed oxidation. The reaction rates were calculated from the slope of the initial part of kinetic plots. Kinetic measurements by circular dichroism were carried out in the same buffer and temperature following the changes of ellipticity at 345 nm. A Cary 61 spectropolarimeter equipped with a termostated sample holder was used.

The reaction was also followed by recording oxygen consumption using a YSI Model 5300 biological oxygen monitor (Yellow Springs Instruments Co., Yellow Springs, OH). The oxygen concentration in air-equilibrated 20 mM phosphate buffer, pH 6.0 at 20 °C, was equal to 0.28 mM. The recorder (LKB 2210 recorder) was calibrated to base line by adding an excess of sodium dithionite to the reaction mixture.

Kinetic experiments at different dioxygen partial pressures were carried out using a tonometer of 250 mL total volume equipped with a quartz cuvette. The Hc solution was equilibrated to the desired dioxygen partial pressure by injecting a known volume of pure dioxygen to the nitrogen atmosphere inside the tonometer, the total pressure being kept constant at 1 atm. The reaction was initiated by injecting a volume (5−20 μL) of N_2-saturated substrate stock solution.

The reaction was also followed by means of the *o*-diphenol-dependent oxidation of *N*,*N*,*N*′,*N*′-tetramethyl-1,4-phenylenediamine dihydrochloride in 20 mM phosphate buffer, pH 6.0 at 20 °C. The process leads to an increase of absorbance at 562 nm corresponding with the absorption maximum of the oxidized species (ϵ = 11 800 M^{-1} cm^{-1}). The molar extinction coefficient of the product was experimentally determined according to Lambert−Beer's equation by fully oxidizing increasing concentrations of the diamine.

In all kinetic experiments, the experimental errors where within ±4%.

HPLC Analysis. HPLC[1] analysis was applied in order to detect and estimate reaction products different from *o*-quinone. Hc (1 mg/mL) was incubated with 2.5 mM *o*-diphenol in O_2-saturated 20 mM phosphate buffer, pH 6.0 (total volume 50 mL). After the increase of absorbance up to 1.2, corresponding to a 0.85 mM quinone solution, 10-fold excess ascorbate was added in order to reduce the quinone. The solution was ultrafiltered on a Pall Filtron device with a 30 kDa cutoff in order to remove Hc and then brought to approximately 2 mL by flask evaporation at room temperature. HPLC analysis was performed with a Perkin-Elmer L-235 instrument using a Lichrom HP-18 reverse-phase column and a UV detector set at 258 nm. A mixture of ethanol (containing 1% acetic acid) and water (v/v ratio 40:60) was used as eluent. Retention times of standards were as follows: *o*-diphenol, 5.4 min; ascorbic acid, 3.7 min; 1,2,3-trihydroxybenzene (THB), 4.3 min; methyl-4-hydroxybenzoic acid (used also as internal standard), 14.3 min; phenol, 7.5 min.

EPR Measurements. Room temperature EPR measurements have been performed under continuous flow conditions in order to produce the steady-state concentrations of paramagnetic species eventually generated during turnover. A Varian EPR spectrometer was used. Two syringes respectively contained the solution of oxy-Hc (4 mg mL^{-1} in 20 mM phosphate buffer, pH 6.0) and the solution of *o*-diphenol (80 mM in the same buffer). The two solutions were continuously mixed in a reaction chamber placed in the magnetic field at a 1:1 (v/v) ratio with the aid of a plunger.

RESULTS

Kinetic and Enzymatic Parameters. Octopus vulgaris Hc is capable of catalyzing the oxidation of *o*-diphenol to the corresponding *o*-quinone. The reaction can be followed by the increase of the absorbance around 400 nm observed upon incubation of the substrate with native oxy-Hc. The correspondence of the reaction product with *o*-quinone has been demonstrated by comparison of the absorption spectrum of the reaction product after extraction with benzene with that of pure *o*-quinone in the same solvent. Both spectra exhibit a single sharp band with a maximum around 390 nm (figure not shown). The *o*-diphenol oxidation does not occur in the absence of dioxygen or with the apo-protein. The time course of the reaction, reported in Figure 1A for different substrate concentrations and with *Octopus* Hc, shows an initial acceleration followed by an almost linear phase and finally a plateau. The limiting absorbance reached at the end of the reaction, however, does not correspond to the complete oxidation of substrate; for instance, in the case of the upper trace (h) of Figure 1A, recorded in the presence of 20.0 mM catechol, the plateau is reached in correspondence of 1 mM quinone. The efficiency of Hc catalysis is very low: in the case above, taking the slope of the quasi-linear portion, it results in 10 mmol of substrate transformed per minute per mole of *Octopus* Hc (M_r = 50K). The dependence of the initial rate of quinone production was studied as function of Hc concentration (with both *Octopus* and *Carcinus* Hcs) and with catechol as substrate. For both proteins, a linear relationship is observed (Figure 1B). The reaction efficiency is much higher with *Octopus* than with *Carcinus* Hc. With methylcatechol, the reaction can still be observed, while upon further increasing the size of the substituent in position 4 on the aromatic ring, the reaction

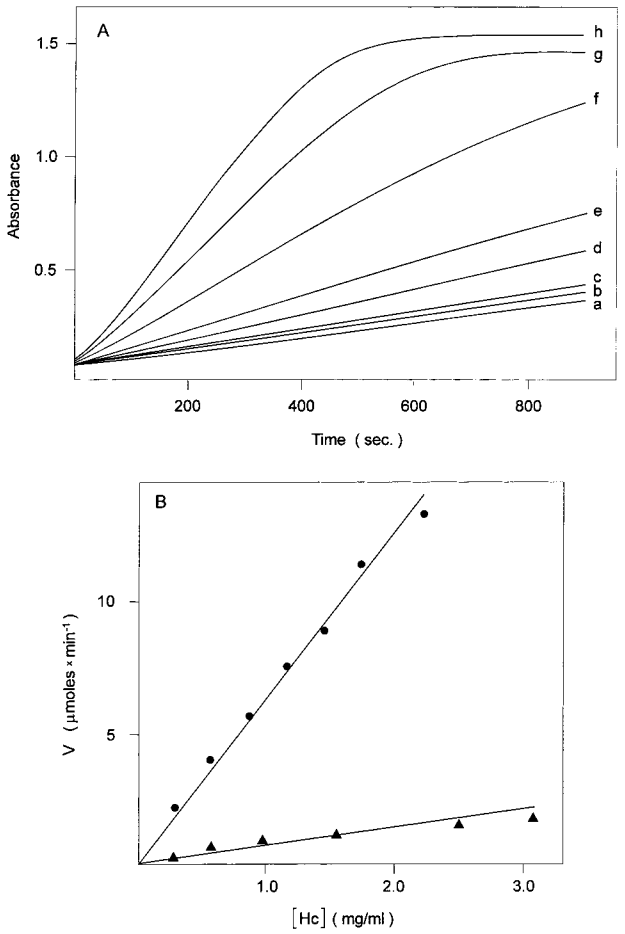

FIGURE 1: Hc-catalyzed oxidation of *o*-diphenol. (A) Time courses of quinone formation in the presence of *Octopus* Hc (1 mg mL^{-1}, 13.3 × 10^{-6} M) and the following different concentrations of *o*-diphenol: (a) 1.3 × 10^{-3} M, (b) 1.7 × 10^{-3} M, (c) 2.0 × 10^{-3} M, (d) 2.7 × 10^{-3} M, (e) 3.3 × 10^{-3} M, (f) 6.7 × 10^{-3} M, (g) 13.3 × 10^{-3} M, (h) 20.0 × 10^{-3} M. (B) Dependence of the rate of quinone formation versus protein concentration. (●) Hc from *Octopus* and *o*-diphenol concentration 0.9 mM; (▲) Hc from *Carcinus* and *o*-diphenol concentration 1.4 mM. Buffer: 20 mM phosphate buffer, pH 6.0, t = 20 °C.

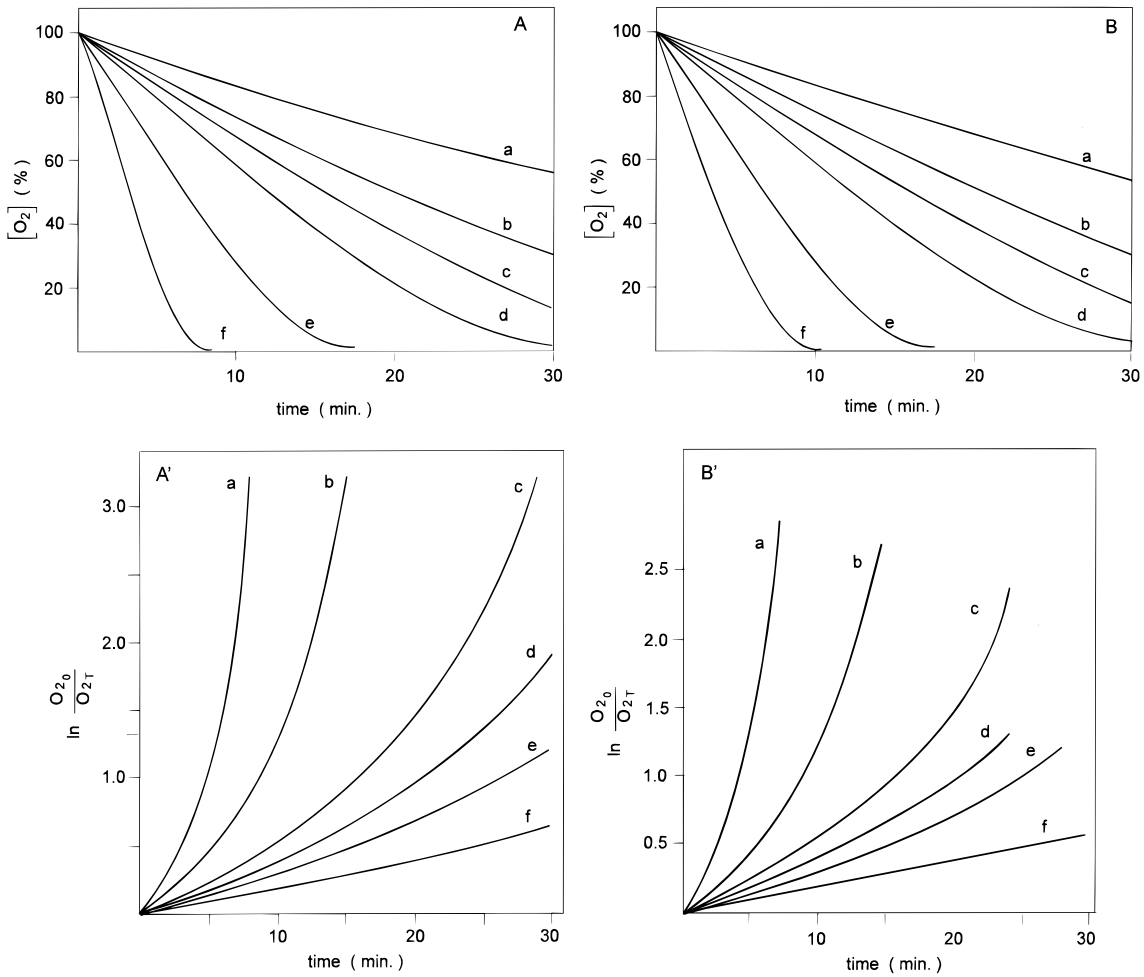

FIGURE 2: Hc-catalyzed oxidation of *o*-diphenol. (A, B) Time courses of oxygen consumption in the presence of *Octopus* Hc (1 mg/mL) and *o*-diphenol (A) or 4-methylcatechol (B) at the following molar concentrations: 1.3×10^{-3} (a), 2.0×10^{-3} (b), 2.7×10^{-3} (c), 3.3×10^{-3} (d), 6.7×10^{-3} M (e), 13.3×10^{-3} (f). In panels A′ and B′, the traces of panels A and B, respectively, are presented in the form of a semilogarithmic plot where O_{2_0} and O_{2_T} are the percent of dissolved dioxygen at time 0 and time after T addition of substrate. Experiments in 20 mM phosphate buffer, pH 6.0, $t = 20$ °C.

rate drastically decreases with both Hcs. No reaction has been observed either with 4-*tert*-butylcatechol or with other monosubstituted *o*-diphenols (caffeine, mimosine, 3,4-dihydroxyphenylalanine, 3,4-dihydroxybenzoic acid, 3,4-dihydroxyphenylacetic acid, 3,4-dihydroxybenzylammonium chloride). The reaction is specific for *o*-diphenols, the corresponding meta and para isomers being unreactive.

In Figure 2A,B, the kinetics of oxygen consumption observed during the oxidation of *o*-diphenols in the presence of costant Hc (from *Octopus*) concentration (2×10^{-5} M) and with substrate (catechol or 4-methylcatechol) concentration ranging from 1 mM to 13.3 mM are shown. In all cases, an almost linear decrease of the physically dissolved oxygen to 20−30% of the starting value is observed, followed by an exponential phase tending asymptotically to zero. The slope of the linear phase increases with substrate concentration. The complex trend followed by oxygen consumption is better evidenced by the semilogarithmic plots of Figure 2A,B, obtained from the traces of Figure 2A,B. An upward curvature, proportional to the substrate concentration, is evident, indicating an apparent acceleration of the process as the reaction proceeds.

The observed involvement of dioxygen in the oxidation reaction suggested an experiment in which the production of quinone is followed spectrophotometrically in a tonometer filled with an atmosphere progressively enriched with dioxygen. The traces reported in Figure 3 are obtained at constant total pressure (1 atm), temperature (21 °C), and substrate (2 mM) and protein (1 mg mL^{-1}) concentrations but when the tonometer contains air (trace a), air plus 20.5% (v/v) pure oxygen (trace b), or pure oxygen (trace c). The initial velocity is the same under all experimental conditions. However, when the kinetics are followed for a relatively long time, it can be seen that the quinone concentration increases up to the plateau value, in correspondence with the consumption of dissolved dioxygen. This is followed by a slow decrease of absorbance. The initial rate of quinone formation is restored after reequilibration of the reaction mixture with the atmosphere inside the tonometer (this step is indicated by the arrow in Figure 3, trace a). The coincidence of the initial reaction rate under the three experimental conditions suggests that the active species is the Hc−peroxide adduct rather than the physically dissolved dioxygen. The concentration of the latter increases 5-fold (from 0.28 mM to 1.37 mM) by changing the atmosphere from air (20.5% O_2) to 100% pure dioxygen; hence, a faster reaction rate is expected in the case of a reaction dependent on physically dissolved dioxygen. On the other hand, the concentration of oxy-Hc

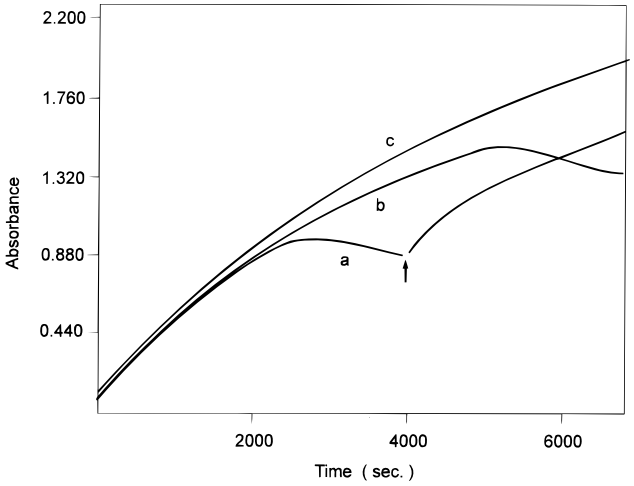

FIGURE 3: Hc-catalyzed oxidation of *o*-diphenol. Time courses of quinone formation in the presence of *Octopus* Hc (1 mg mL^{-1}) and *o*-diphenol (2.0 mM) in 20 mM phosphate buffer, pH 6.0, equilibrated in (a) air, (b) 0.61 mM oxygen, and (c) pure oxygen at 20 °C. The arrow indicates successive equilibration of the reaction mixture with the air inside the tonometer.

is almost unchanged since the protein is already ≈75% saturated in air (the ratio A_{340}/A_{278} at pH 6.0 is 0.19). No significant changes in the reaction rate are, therefore, expected in the case of a reaction involving bound peroxide.

To further sustain this point, the initial rate of quinone production has been measured under conditions in which Hc and catechol concentrations are kept constant ([Hc] = 1 mg mL^{-1}, 20 μM, and [*o*-diphenol] = 1.2 mM), the dioxygen pressure changing between 10 and 610 mmHg. Figure 4A shows that the reaction rate increases with the initial pressure of dioxygen following a hyperbolic trend with an asymptotic value of velocity (0.027 μmol min^{-1} mg^{-1}). This plot closely resembles the dioxygen equilibrium curve of *Octopus* Hc under the same experimental conditions. In Figure 4B, the data are presented as a Hill plot where the fractional saturation of the protein with dioxygen is calculated on the basis of the fractional reaction velocity for each pO_2 with respect to the asymptotic velocity. The straight line has a slope $n = 1$ and an apparent equilibrium constant for dioxygen of 0.08 mM, very close to the value of 0.09 mM measured from the oxygen equilibrium curve.

The involvement of oxy-Hc in the catalytic function is further confirmed by measuring the changes of oxy-Hc concentration during turnover. For this measurement, one can take advantage of the strong negative ellipticity of the copper−peroxide absorption band, with the maximum near 340 nm, and of the fact that neither catechol nor *o*-quinone are optically active. The traces reported in Figure 5 represent the time dependence of the decrease of negative ellipticity at 345 nm due to oxy-Hc, superimposed to the increase of absorbance due to the reaction product. The consumption of oxy-Hc is much slower than quinone formation and suggests that this Hc species is in steady-state and is indeed regenerated during turnover, the decrease of its concentration resulting from consumption of dioxygen in the bulk solution.

In Figure 6 the Lineweaver−Burk plots obtained for *Octopus* Hc on the basis of quinone production or of oxygen consumption are reported (S being *o*-diphenol, Figure 6A, or 4-methylcatechol, Figure 6B). The intercepts obtained by interpolating the straight lines according to the least-squares method are very small, and the corresponding values of K_M and V_{max} relative to quinone formation are 35 mM and 0.37 mmol min^{-1} for *o*-diphenol and 50 mM and 0.45 mmol min^{-1} for methylcatechol, respectively. Comparison between the quinone production and the oxygen consumption rates measured under the same experimental conditions allowed us to calculate the stoichiometric ratio between quinone produced to oxygen consumed as 2:1.3 (Figure 7), significantly lower than the 2:1 stoichiometry found with Ty. The plot of Figure 7 is essentially linear over the whole range of substrate concentrations because catechol is kept far below the formal K_M value.

Generation of Radical Species. The oxidation of *o*-diphenol to quinone produces as intermediate species *o*-semiquinone radicals, detectable by EPR spectroscopy under flow conditions (Figure 8). The intensity of the spectrum is compatible with the hypothesis that the radical species is the product of the first step of the interaction between oxy-Hc and *o*-diphenol.

The production of semiquinone radicals is confirmed using *N*,*N*,*N*′,*N*′-tetramethyl-1,4-phenylenediamine. This compound is known to undergo monoelectronic oxidation by suitable electrophilic free radicals to yield a stable cationic free radical species exhibiting an intense characteristic

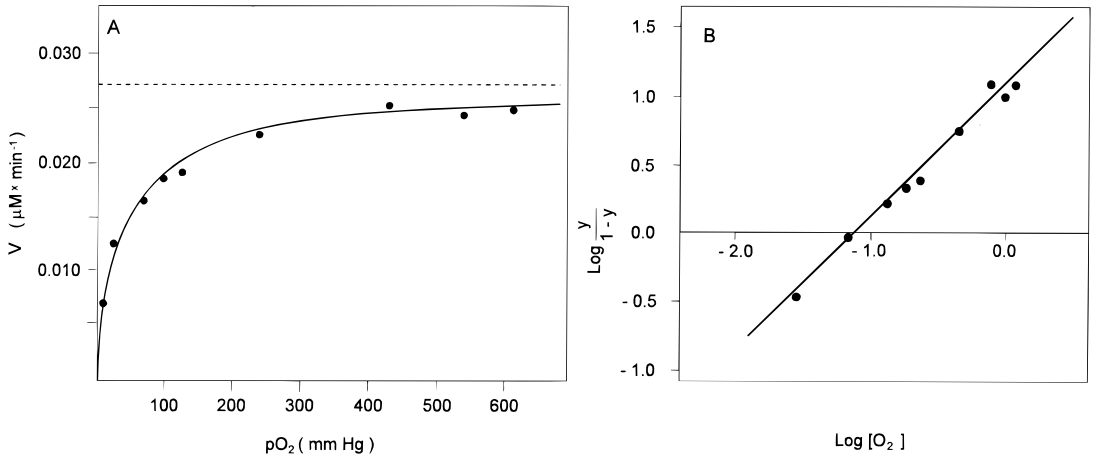

FIGURE 4: Oxidation of *o*-diphenol catalyzed by *Octopus* Hc. (A) Dependence of the reaction rate versus oxygen partial pressures. The dashed line represents the asymptotic maximum velocity. (B) Data as in (A) reported in the form of a Hill plot. [Hc] = 1 mg mL^{-1}, [*o*-diphenol] = 1.2 mM, 20 mM phosphate buffer, pH 6.0, t = 20 °C.

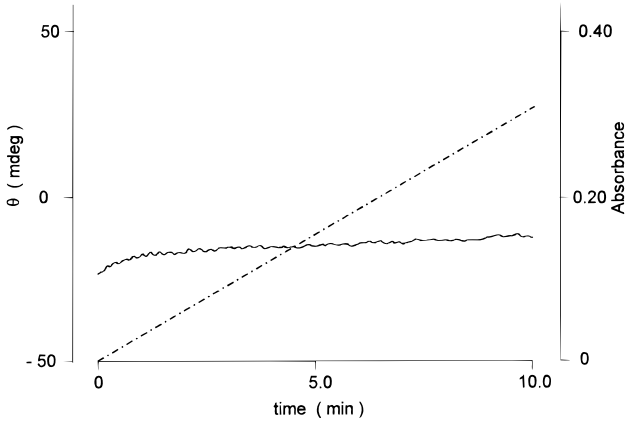

FIGURE 5: Hc-catalyzed oxidation of *o*-diphenol. Time dependence of ellipticity at 340 nm of oxy-Hc (lower continuous trace, left *y*-axis); absorbance at 400 nm of quinone produced (dotted−dashed trace, first right *y*-axis). [Hc] = 3.4 mg mL^{-1} [*o*-diphenol] = 0.4 mM.

absorption band at 562 nm (ϵ = 11 800 M^{-1} cm^{-1}). In Figure 9 the initial rate of formation of the cationic radical is reported as a function of *o*-diphenol concentration in the presence of oxy-Hc. No reaction has been observed in the absence of *o*-diphenol or in the absence of oxy-Hc. In the same figure, the initial rate of quinone formation, under the same experimental conditions, is also reported. In both cases, linear plots are obtained, the catechol concentration being kept below K_M, and comparison of the slopes shows that the initial rate of *N*,*N*,*N*′,*N*′-tetramethyl-1,4-phenylenediamine radical formation is about 2 times higher than the initial rate of quinone formation. This result is in agreement with the hypothesis that the first step of *o*-diphenol oxidation by oxy-Hc actually produces a semiquinone radical, which in turn generates quinone upon dismutation.

HPLC Analysis. The stoichiometric data on quinone produced per dioxygen consumed (see above) suggested that, in addition to quinone, other products must be formed during catalysis, thus decreasing the yield of quinone formed with respect to oxygen consumed. Therefore, we performed an HPLC analysis of the reaction mixture, quenched by the addition of excess ascorbic acid and after removal of the protein by ultrafiltration. Ascorbic acid was introduced in order to prevent further reactions of quinones and to regenerate the phenols that are more easily analyzed by HPLC.

In addition to the expected peaks corresponding to *o*-diphenol and ascorbic acid, the HPLC traces show two additional peaks. The first peak at 4.3 min could be assigned, by reference with a standard sample, to 1,2,3-trihydroxybenzene (THB)[1] while another peak with a retention time of 6.8 min is assigned to some other product. Quantitation of the THB peak indicates it corresponds to about 5% mol equiv with respect to *o*-diphenol. For the peak at 6.8 min, assuming its detector response is similar to that of *o*-diphenol, an estimate of about 10% mol equiv with respect to catechol can be made.

Reactions of Oxidized Hc Derivatives. The semi-oxidized form of Hc (semi-met-Hc) containing a [Cu^{II}Cu^{I}] active site does not react with *o*-diphenols. The fully oxidized or dicupric form (met-Hc) oxidizes the substrates with an efficiency comparable to the native form (Figure 10A). Noteworthy, quinone formation occurs in a single cycle and in a 1:1 stoichiometric ratio with respect to the protein concentration when the reaction is carried out with met-Hc anaerobically. These observations indicate that met-Hc is reduced by *o*-diphenol to deoxy-Hc that, in turn, initiates the catalytic turnover only in the presence of air by binding dioxygen. In agreement, the incubation of met-Hc with catechol in a CO atmosphere results in the appearance of the typical luminescence spectrum of the adduct of CO with deoxy-Hc (Figure 10B) documenting the reduction of met-Hc to the deoxy form, concomitant to *o*-diphenol oxidation (the low emission intensity observed with met-Hc before treatment with *o*-diphenol is attributable to the presence of a small fraction of deoxy-Hc present in the met-Hc sample).

DISCUSSION

The functional cycle of Hc, involving coordination of dioxygen to the dinuclear copper site, results in the activation of the ligand as a consequence of metal-to-dioxygen electron transfer. Thus, in addition to the oxygen transport and/or storage function, it is conceivable that Hc exhibits other

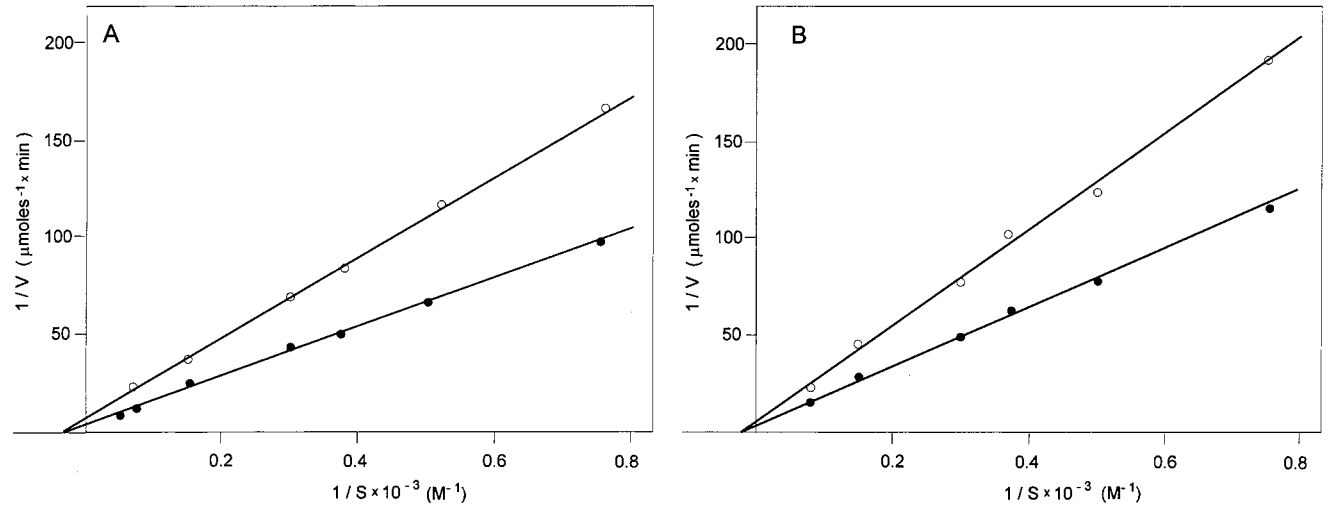

FIGURE 6: Hc-catalyzed oxidation of *o*-diphenol. Lineweaver−Burk plots from the data of quinone production (●) and from the data of oxygen consumption (○). Substrates: *o*-diphenol (A), 4-methylcatechol (B). [Hc] = 1 mg mL^{-1}, 20 mM phosphate buffer, pH 6.0, t = 20 °C.

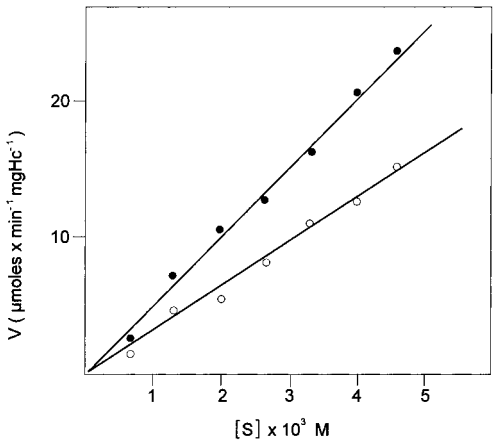

FIGURE 7: Hc-catalyzed oxidation of *o*-diphenol. Dependence of the reaction velocity as a function of substrate concentration. The reaction is followed by means of quinone production (●) and oxygen consumption (○). Protein concentration and experimental conditions as in Figure 1.

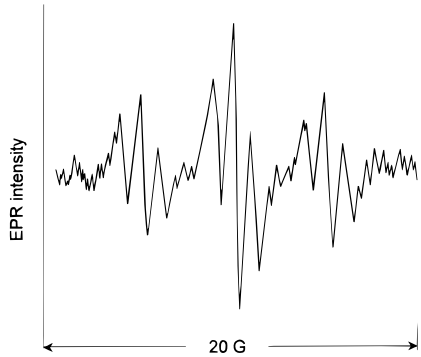

FIGURE 8: Room-temperature EPR spectrum recorded by continuous mixing solutions of Hc and catechol. Modulation, 4 × 0.1 G. For details, see Materials and Methods.

reactivities in the presence of suitable exogenous molecules. In this frame, the capability of Hcs to catalyze *o*-diphenol oxidation to the corresponding quinones has to be considered as a side property of the metal−dioxygen active site adduct. This reaction is, however, worth studying because it provides useful information for a deeper understanding of the bioinorganic chemistry of the copper dinuclear site of this class of proteins.

Several observations show that oxy-Hc is the active species directly interacting with the substrate. The trend of kinetic plots describing the time dependence of quinone formation is consistent with the involvement of dioxygen as cosubstrate, but it does not allow us to discriminate between the physically dissolved or Hc-bound dioxygen. In the same line are the results of the reintroduction of dioxygen when the reaction reached the plateau and also the dependence of the position of the plateau itself as a function of the initial oxygen partial pressure. When the reaction is followed from the oxygen consumption rate, its kinetics can easily be explained by assuming that the reaction is consuming the physically dissolved dioxygen only through oxy-Hc. In the case of *Octopus* Hc, under our experimental conditions, the fraction of the oxygenated form is a hyperbolic function of pO_2. The close similarity between the oxygen binding curve and the curve obtained by plotting the initial rate of quinone formation as a function of pO_2 demonstrates that the active form is oxy-Hc and that dioxygen is brought into the catalytic

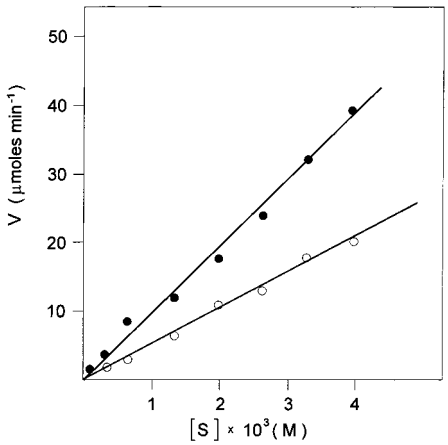

FIGURE 9: Hc-catalyzed oxidation of *o*-diphenol. Dependence of the reaction velocity as a function of substrate concentration. The reaction is followed by means of quinone production (○) and oxidation of *N*,*N*,*N*′,*N*′- tetramethyl-1,4-phenylenediamine hydrochloride (●). Conditions: [Hc] = 1 mg/mL, [*N*,*N*,*N*′,*N*′-tetramethyl-1,4-phenylenediamine] = 0.33 mM in 20 mM phosphate buffer, pH 6.0, t = 20 °C.

cycle only upon binding to deoxy-Hc. Thus, the concentration of oxy-Hc is expected to remain under turnover conditions unless the physically dissolved oxygen becomes a limiting factor. The CD[1] data obtained on the negative band of oxy-Hc confirm this hypothesis.

The efficiency of oxidation is very low as indicated by the small intercepts of Lineweaver−Burk plots typical for a system with low affinity and high V_{max}.

According to the crystallographic model of arthropod Hc (*2*) the active site is deeply embedded into the protein matrix, and the low affinity for the substrate can be proposed to result from steric hindrance to reach the active site. In line with this hypothesis are the results on the specificity of the reaction as a function of the presence of substituents in position 4 of *o*-diphenol. The vicinity of the two hydroxyl groups is a determinant for the reaction as demonstrated by the lack of reaction for 1,3- and 1,4-diphenols. The importance of active site accessibility in controlling the reaction rate results also by comparing the efficiency of different Hcs. *Octopus* Hc is far more efficient than *Carcinus* Hc, as expected on the basis of previous results on the interaction with CN^- showing that the former protein has a much more exposed active site (*14*). It is worth noting that the addition of perchlorate, an agent known to perturb protein conformation by increasing the active site accessibility of *Carcinus* Hc (*22*), to the reaction medium increases the reaction efficiency of the same Hc (*17, 23*). Furthermore, the dissociated subunit of *Carcinus* is far more efficient than the aggregated whole molecule (*17*).

Several experimental results point to a reaction mechanism different from that proposed for Ty (*10, 24*). The oxygen consumption curves of Ty, recorded during oxidation of *o*-diphenols, show the occurrence of an inhibition reaction resulting in the loss of enzymatic activity and modification of the active site (*10, 24*); in contrast, Hc consumes all dioxygen available (Figure 2A). Flow EPR measurements allow identification of a semiquinone radical as the first intermediate in the oxidation reaction with Hc. The results obtained with *N*,*N*,*N*′,*N*′-tetramethyl-1,4-phenylenediamine show that the production of radical occurs at a rate 2-fold

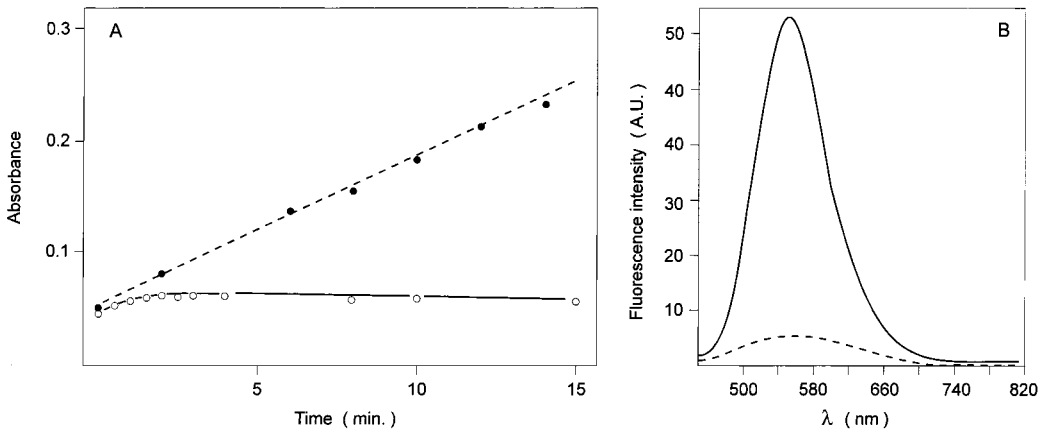

FIGURE 10: (A) Oxidation of *o*-diphenol (1.2 mM) by met-Hc (1 mg mL^{-1}) in a nitrogen atmosphere (○, solid line) and in air (●, dashed line). (B) Emission spectrum of Hc (excitation at 295 nm) under CO atmosphere before (dashed line) and after (solid line) addition of 1.2 mM *o*-diphenol.

higher than that of quinone. It can be, therefore, concluded that the quinone is not the primary product of the reaction with Hc as it would occur in a bielectronic process similar to that proposed for Ty, but it depends on the dismutation of semiquinone radicals, the primary products of a monoelectronic process.

As far as the mode of substrate interaction is concerned, we propose that it occurs through bound peroxide rather than through copper. Supporting this view are the results of crystallographic data on arthropod Hc. Although there is formally an open axial coordination position for exogenous ligands to the copper, this is oriented toward the opposite side with respect to the binuclear site, thus precluding simultaneous coordination of the two hydroxyl groups of catechol to the metal ions, as formerly proposed in the case of Ty (*10*, *11*, *24*). In addition, polarographic experiments (*25*) have shown that in oxy-Hc the accessible surface of the active site is the bound peroxide. It is also conceivable that this electron-rich peroxide extracts hydrogen homolytically from the hydroxyl groups of *o*-diphenol, thus leading to semiquinone radical formation. In contrast, it has been shown that the active site of Ty is highly accessible to substrate analogues which bind directly to the copper center (*11*, *26*).

On the basis of our experimental evidence, we propose the reaction mechanism given below where the global oxidation numbers of the complex between dinuclear copper and activated oxygen ligand are accounted for (Scheme 1). The scheme is reduced to the five steps that account for the generation of protein redox intermediates and does not include transient species coordinating catechol. A more detailed description is given in the Appendix where the model is solved kinetically.

In this scheme, in addition to a first step consisting of the reversible binding of dioxygen (step 1) to deoxy-Hc [Cu^{I}-Cu^{I}] to yield oxy-Hc [$Cu^{II}O_2^{2-}Cu^{II}$], the reaction is initiated by the interaction of *o*-diphenol (catechol, C) with Hc-bound peroxide to give an activated adduct, HcO_2C. This decomposes into a semiquinone radical (S^{o}) and a species (HcO_2H) corresponding formally to a protein intermediate containing a dinuclear Cu(I) site like deoxy-Hc with a superoxide [Cu^{I}-($O_2H^{\bullet}$)Cu^{I}], or a met-Hc form with a hydroxyl radical [$Cu^{I}(OH^{\bullet})(OH^{-})Cu^{I}$] (step 2). This further reacts with a second *o*-diphenol molecule either to give S° again and a

Scheme 1

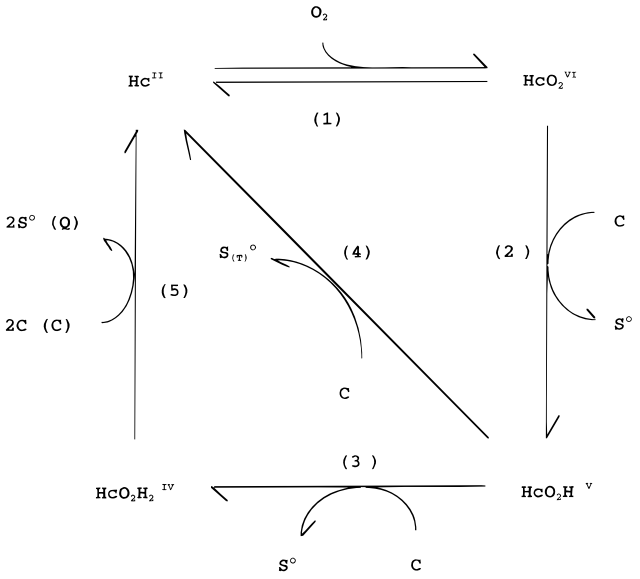

species (HcO_2H_2) corresponding formally to deoxy-Hc with peroxide or met-Hc [$Cu^{II}(OH^{-})_2Cu^{II}$] (step 3) or to produce a triphenol radical, $S_{(T)}^{\circ}$, and deoxy-Hc by *o*-diphenol hydroxylation, in a formal three-electron process that may proceed through several steps (step 4). The HcO_2H_2 species reacts formally in a bielectronic process with *o*-diphenol to give deoxy-Hc (Hc) and a quinone molecule (Q) (step 5, substrate and product in parentheses); the former regenerates the active oxy-Hc species by binding physically dissolved dioxygen (step 1). Quinone, therefore, results from both the latter reaction and the dismutation of semiquinone radicals. Step 5 deserves further comments: it involves the direct formation of *Q*; thus, the overall semiquinone-to-quinone stoichiometry would be 1:1. However, *N*,*N*,*N*′,*N*′-tetramethyl-1,4-phenylendiamine experiments show that the ratio of semiquinone-to-quinone formation rates is 2:1. This step, therefore, can be written as two sequential monoelectronic steps (see Appendix) in which met-Hc is likely to be reduced first to semi-met-Hc [$Cu^{II}Cu^{I}$] and then to deoxy-Hc. The results reported in Figure 10 demonstrate that met-Hc can be converted to deoxy-Hc by the substrate. In contrast, semi-met-Hc could not be reduced by *o*-diphenol. This semi-met derivative, however, represents a ligated protein derivative in which the copper-bound ligand is likely to compete with

the substrate, and, therefore, the possibility that met-Hc is reduced through two successive monoelectronic steps cannot be ruled out. Step 4 is included to account for the noninteger ratio between the rate of quinone formation versus O_2 consumption (2:1.3), the formation of trihydroxybenzene (THB) being confirmed by reverse-phase HPLC. By this approach, we have shown the presence of other product(s) beside THB. Even though the other product is not identified, its retention time (6.8 min), intermediate between that of phenol (7.5 min) and *o*-diphenol (5.4 min), suggests a less polar structure with respect to either THB or *o*-diphenol. This suggests that it might result from dimerization or further oligomerization of the radical products.

It is worth noting that in the absence of step 4, the quinone-to-dioxygen stoichiometry would be the same as for a purely bielectronic process (2:1), while the *o*-diphenol-to-quinone ratio is always formally 1:1 both in the presence and in the absence of step 4. The direct reduction of met-Hc by *o*-diphenol and its reconversion to oxy-Hc by binding dioxygen experimentally sustain step 5.

The reaction scheme described above has been mathematically treated (see Appendix), and the kinetic equations obtained were used to simulate the data of oxygen consumption. The continuous lines in Figure 1B representing the experimental traces are almost superimposed with the curves generated according to the model. It is important to underline that in such experiments *o*-diphenol is in large excess (1.3−13.3 mM) with respect to dioxygen (0.28 mM); hence, the reaction is never limited by this substrate. The description of the kinetics of quinone formation is more entangled because the dioxygen concentration cannot be considered constant, being lower than the substrate concentration, and this drastically limits the reaction before *o*-diphenol is consumed (see Appendix).

Strong similarities exist between the active sites of Hc and tyrosinase, two proteins phylogenetically related (*27*−*29*) although performing quite different physiological roles. The tyrosinase-like activity of Hc is peculiar not only for its low efficiency but also as far as the reaction mechanism is concerned. In the case of Ty, a reaction scheme was proposed based on concomitant binding of the substrate and peroxide at the dinuclear copper site (*10, 30*). In the case of Hc, our experimental evidence suggests that the substrate interacts with the Hc-bound peroxide; the process is monoelectronic, and the oxidation proceeds following a radical mechanism. The mechanism proposed for Hc also allows explanation of some peculiarities of the reaction in comparison with the behavior of Ty. In particular, the ratio between dioxygen consumed and quinone produced is noninteger (1.3:2), in contrast to tyrosinase (1.0:2). The difference is largely significant, being the standard error of the slopes of the straight lines of Figure 7 within ±4%. Furthermore, Hc does not undergo the inactivation reaction typical of the Ty-catalyzed *o*-diphenol oxidation (*10*).

In addition to the intrinsic electronic factors that are likely to affect the reactivity of the copper−peroxide active site of Ty and Hc (*30*), hence differentiating the biological role of the two proteins, our results point to the importance of steric factors. The elucidation of the tyrosinase gene sequence of *Neurospora crassa* has revealed that the protein is synthesized in the form of a precursor protein with a C-terminal elongation of 213 amino acids as compared to the mature enzyme. This region shows distinct similarities with the C-terminal part of arthropod Hc (domain 3) folded as to form a β-barrel shielding the active site (*31*).

Scheme 2

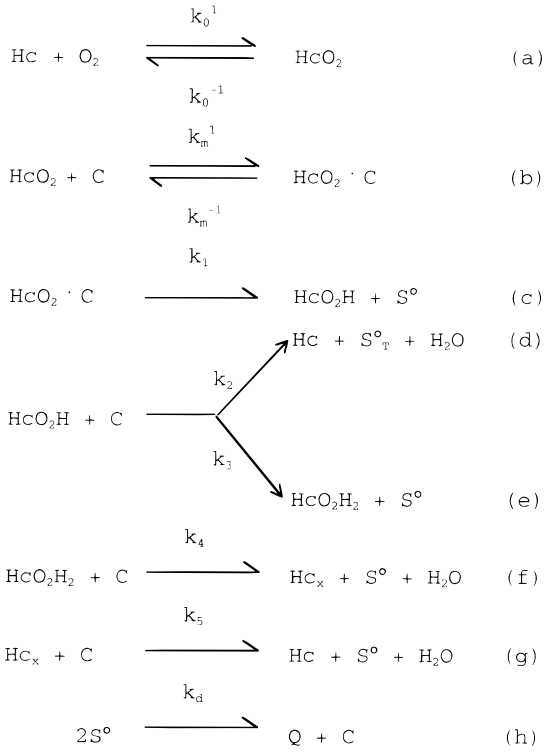

The coordination of dioxygen as peroxide in a dinuclear copper active site as it is found in Ty and Hc has the ultimate effect of activating the ligand with respect to redox reactions involving *o*-diphenols. The high accessibility of the Ty active site to exogenous molecules allows the interaction with bulky substrates; in contrast, the low active site accessibility of Hc allows coordination to copper of molecules only as small as dioxygen. These steric effects are expected to play an important role in modulating the catalytic efficiency by affecting the accessibility of the active site toward exogenous molecules. Thus, the catecholase activity exhibited by molluscan and arthropod Hcs has to be considered a property of the protein resulting from the peculiar coordination of dioxygen, strictly controlled by the low accessibility of the active site to substrate molecules. This activity of Hc, therefore, can be considered as an intrinsic property of the copper−peroxide adduct still maintained after the functional divergence of Hc from the more ancient tyrosinase.

ACKNOWLEDGMENT

The excellent technical assistance of Mr. G. P. Rocco and A. Cervellin for the preparation of hemocyanin is gratefully acknowledged.

APPENDIX

In this appendix, we describe the solution of a kinetic model that simulates the experimental curves of quinone formation and oxygen consumption during the reaction of Hc with *o*-diphenol. The model is based on the reaction scheme whose experimental evidences are discussed above (Scheme 2).

Equations a and b concern the binding equilibria of deoxy-Hc with oxygen and of oxy-Hc with *o*-diphenol, respectively. Equations c−f refer to the decomposition of the Hc−*o*-diphenol adduct and of its intermediates to give deoxy-Hc; each step produces a semi-quinone radical of *o*-diphenol (S°) and, in one instance (eq d with rate constant k_2), of THB (S°_T). In the latter case, an ortho-hydroxylation reaction occurs together with radical formation. From HPLC analysis, it is demonstrated that beside THB another product is formed, characterized by marked hydrophobicity. This event is not considered in Scheme 2 because THB can be considered for simplicity the only alternative step to semiquinone formation. According to eq h, the quinone arises from the dismutation of the semi-quinone radicals. Dioxygen enters into the catalytic cycle only through oxy-Hc, its reduction occurring exclusively within the Hc active site.

According to the proposed reaction scheme, a system of differential equations describing the rate of appearance of the various intermediates (eqs 1−10) can be written, together with a mass equation (eq 11) which accounts for the distribution of the total Hc between the various intermediates:

$$\frac{d[O_2]}{dt} = -k_0^1[Hc][O_2] + k_0^{-1}[HcO_2] \quad (1)$$

$$\frac{d[HcO_2]}{dt} = k_0^1[Hc][O_2] - k_0^{-1}[HcO_2] - k_m^1[HcO_2][C] + k_m^{-1}[HcO_2C] \quad (2)$$

$$\frac{d[HcO_2C]}{dt} = k_m^1[HcO_2][C] - k_m^{-1}[HcO_2C] - k_1[HcO_2C] \quad (3)$$

$$\frac{d[HcO_2H]}{dt} = k_1[HcO_2C] - (k_2 + k_3)[HcO_2H][C] \quad (4)$$

$$\frac{d[HcO_2H_2]}{dt} = k_3[HcO_2H][C] - k_4[HcO_2H][C] \quad (5)$$

$$\frac{d[Hc_x]}{dt} = k_4[HcO_2H_2][C] - k_5[Hc_x][C] \quad (6)$$

$$\frac{d[Hc]}{dt} = -k_0^1[Hc][O_2] + k_0^{-1}[HcO_2] + k_2[HcO_2H][C] + k_5[Hc_x][C] \quad (7)$$

$$\frac{d[S^\circ]}{dt} = k_1[HcO_2C] + (k_2 + k_3)[HcO_2H][C] + k_4[HcO_2H_2][C] + k_5[HC_x][C] - 2k_d[S^\circ]^2 \quad (8)$$

$$\frac{d[C]}{dt} = -k_m^1[HcO_2][C] + k_m^{-1}[HcO_2C] - (k_2 + k_3)[HcO_2H][C] - k_4[HcO_2H_2][C] - k_5[Hc_x][C] + k_d[S^\circ]^2 \quad (9)$$

$$\frac{d[Q]}{dt} = k_d[S^\circ]^2 \quad (10)$$

$$[Hc]_{total} = [Hc] + [HcO_2] + [HcO_2C] + [HcO_2H] + [HcO_2H_2] + [Hc_x] \approx [Hc] + [HcO_2] + [HcO_2H] \quad (11)$$

The application of the steady-state approximation to the above system allows obtainment of simpler differential and mass equations suitable to be integrated to give the time course of some reactants and reaction products which can be experimentally determined.

The sum of eqs 1−3, under the steady-state approximation, gives eq 12:

$$\frac{d[O_2]}{dt} + \frac{d[HcO_2]}{dt} + \frac{d[HcO_2C]}{dt} = -k_1[HcO_2C] \quad (12)$$

reduced to

$$\frac{d[O_2]}{dt} = -k_1[HcO_2C] \quad (13)$$

being

$$\frac{d[O_2]}{dt} \gg \frac{d[HcO_2]}{dt} + \frac{d[HcO_2C]}{dt}$$

With the same procedure, we obtain from eqs 4−10:

$$\frac{d[Q]}{dt} = k_1\left(\frac{k_3}{k_2 + k_3} + 1\right)[HcO_2C] \quad (14)$$

describing the time course of quinone formation. By combining eqs 13 and 14:

$$\frac{d[Q]}{d[O_2]} = -\left(\frac{k_3}{k_2 + k_3} + 1\right) \quad (15)$$

Equation 15 represents the ratio between the rate of quinone production and that of oxygen consumption; its value is limited between 1 and 2 depending upon the relative values of k_2 and k_3, namely, on the relative weight of reactions d and e of Scheme 2. It is worth noting that from eq 15, when $k_3 \gg k_2$, the value of $d[Q]/d[O_2]$ approaches 2, which corresponds to that of a formally bielectronic process, as in the case of tyrosinase. A noninteger stoichiometry results from reaction d responsible for the accumulation of the triphenol detected by HPLC.

The kinetics of oxygen consumption can be analytically described by integrating eq 13 and considering a reduced mass law for the total concentration of Hc having the form:

$$[Hc]_{total} \approx [Hc] + [HcO_2] + [HcO_2C] = \text{constant}$$

because the concentration of other protein species can be considered negligible.

Since

$$[Hc] = \frac{K_0[HcO_2]}{[O_2]}; \quad [HcO_2] = \frac{K_m[HcO_2C]}{[C]}; \quad K_0 = \frac{k_0^1}{k_0^{-1}}; \quad K_m = \frac{k_m^1}{k_m^{-1}}$$

it follows that

$$[Hc]_{tot} = \frac{K_0K_m}{[C][O_2]}[HcO_2C] + \frac{K_m}{[C]}[HcO_2C] + [HcO_2C]$$

namely:

$$[HcO_2C] = \frac{[Hc]_{tot}}{(K_m/[C])(K_0/[O_2] + 1) + 1} \quad (16)$$

This result allows generation from eq 13 of the following differential equation:

$$\frac{d[O_2]}{dt} = -k_1[Hc]_{tot}\frac{[C][O_2]}{K_mK_0 + (K_m + [C])[O_2]} \quad (17)$$

or

$$\left(\frac{K_mK_0}{[Hc]_{tot}[C][O_2]} + \frac{K_m + [C]}{[Hc]_{tot}[C]}\right)d[O_2] = -k_1dt \quad (17')$$

having the general form

$$a\,dx/x + \beta\,dx = g\,dt$$

Assuming that [C] is constant, being in large excess with respect to $[O_2]$, the equation can be integrated between time $t = 0$ ($[O_2]_0$) and t($[O_2]_t$) to yield

$$\frac{K_mK_0}{[Hc]_{tot}[C]}\ln\frac{[O_2]_0}{[O_2]_t} + \frac{K_m + [C]}{[C][Hc]_{tot}}([O_2]_0 - [O_2]_t) = k_1t \quad (18)$$

or

$$\ln\frac{[O_2]_0}{[O_2]_t} + Y[(O_2]_0 - [O_2]_t) = Wt \quad (18')$$

where Y and W are respectively equal to

$$Y = \frac{1}{K_0}\left(1 + \frac{[C]}{K_m}\right) \text{ and } W = \left(\frac{[Hc]_{tot}k_1}{K_0K_m}\right)[C]$$

A similar procedure can be followed to obtain the time course of quinone production at constant concentration of oxygen, taking into account that (see eq 14)

$$\frac{d[Q]}{dt} = -\frac{d[C]}{dt} = k_1\left(\frac{k_3}{k_2 + k_3} + 1\right)[HcO_2C] = k^*[HcO_2C]$$

and that $[HcO_2C]$ depends on *o*-diphenol concentration as indicated in eq 16.

The differential equation, analogous to eq 17′, is

$$\left[\frac{K_m(K_0 + [O_2])}{[O_2]}\frac{1}{[C]} + 1\right]d[C] = -k^*[Hc]_{tot}\,dt \quad (19)$$

The integrated equation is

$$\ln\frac{[Q]_\infty}{[Q]_\infty - [Q]_t} + \frac{[O_2]}{K_m(K_e + [O_2])}[Q]_t = \frac{k^*[Hc]_{tot}[O_2]}{K_m(K_e + [O_2])}t \quad (19')$$

where k^* is

$$k^* = k_1\left(\frac{k_3}{k_2 + k_3} + 1\right)$$

and $[Q]_t$ and $[Q]_\infty$ represent the quinone concentration at time t and at infinite time, respectively. $[Q]_\infty$ is equal to the concentration of time 0 of *o*-diphenol, $[C]_0$. The combination of eqs 13, 16, and 17 gives

$$\ln\frac{[Q]_\infty}{[Q]_\infty - [Q]_t} + aY[Q]_t = Wt \quad (20)$$

where

$$a = \left(\frac{k_3}{k_2 + k_3} + 1\right)^{-1}$$

Both Y and W contain [C], and the plots $Y = f([C])$ and $W = f([C])$ allow the evaluation of k_1 and K_m, K_0 being independently calculated from oxygen binding experiments ($K_0 = 0.09$ mM). Furthermore, both eqs 18 and 20 contain W; thus, k_1 and K_m can be calculated from kinetic measurements of oxygen consumption and quinone formation. The plots of W versus substrate concentration are shown in Figure 11 for *o*-diphenol (panel A) and methylcatechol (panel B). The obtained values of k_1 and K_m constants are $k_1 = 0.19$ s^{-1}, $K_m = 27$ mM with *o*-diphenol and $k_1 = 0.18$ s^{-1}, $K_m = 39$ mM with methylcatechol. By comparing these constants, it can be concluded that the different efficiency of substrate oxidation (*o*-diphenol versus 4-methylcatechol) does not depend on the formal first-order rate of electron transfer (k_1)

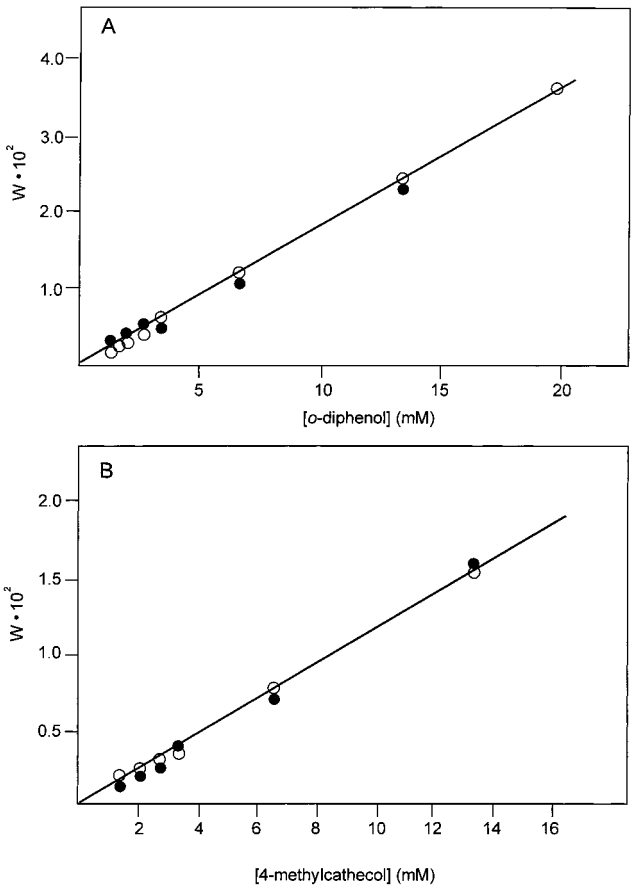

FIGURE 11: Determination of K_m and k_1 values from the kinetic analysis. Equations 18 and 20 reported in the Appendix have been applied to kinetic curves of oxygen consumption (●) and quinone formation (○) obtained in the presence of (A) *o*-diphenol and (B) 4-methylcatechol.

but on the different equilibrium constant exhibited by Hc for the two substrates (K_m).

Equation 18 (or 18′) has been obtained under the steady-state approximation and, hence, is not suitable to fit the initial time of the reaction. This period consists of a lag phase which can be seen both in quinone production and in oxygen consumption. In order to get an equation describing the initial production of quinone, eq 8 can be rewritten in the following compact form:

$$\frac{d[S^\circ]}{dt} = 2K_i[Hc_x]_i - 2k_d[S^\circ]^2 \qquad (21)$$

where $2K_i[Hc_x]_i$ stands for $k_1[HcO_2C] + ... + k_5[Hc_x][C]$ of eq 8. Furthermore, by considering

$$k^* = \left(\frac{2K_i[Hc_x]_i}{k_d}\right)^{1/2}$$

one obtains

$$\frac{d[S^\circ]}{k^{*2} - [S^\circ]^2} = 2k_d\, dt \qquad (21')$$

Integrating eq 21′:

$$\ln\frac{k^* + [S^\circ]}{k^* - [S^\circ]} = 4k^*k_d t = k'' t \qquad (22)$$

$$[S^\circ] = k^*\frac{e^{k''t} - 1}{e^{k''t} + 1} \qquad (23)$$

Similarly, as far as quinone production is concerned:

$$\frac{d[Q]}{dt} = k_d(k'')^2\left(\frac{e^{k''t} - 1}{e^{k''t} + 1}\right)^2 \qquad (24)$$

$$[Q] = k^*\left(\frac{1}{1 + e^{k''t}} + \frac{k''t}{4} - \frac{1}{2}\right) \qquad (25)$$

Equations 23 and 25 describe the time dependence of the semiquinone and quinone concentrations, respectively. Equation 24 describes the time dependence of the rate of quinone production. In Figure 12, the results of such simulations (eqs 23−25) are shown: the dependence of quinone production from the preliminary formation of semiquinone is simulated by both the lag of the curve relative to the time dependence of the former species and the acceleration of the reaction velocity.

Equation 17 can be arranged in a form giving a linear Lineweaver−Burk plot for oxygen consumption, with $V = -d[O_2]/dt$, $V_{max} = k_1[Hc]_{tot}$, and

$$K_m' = K_m\left(\frac{K_0}{[O_2]} + 1\right)$$

$$\frac{1}{V} = \frac{K_m'}{V_{max}}\frac{1}{[C]} + \frac{1}{V_{max}} \qquad (26)$$

Similarly, from eq 14 substituting $V'_{max} = k_1[Hc]_{tot}/a$, one obtains

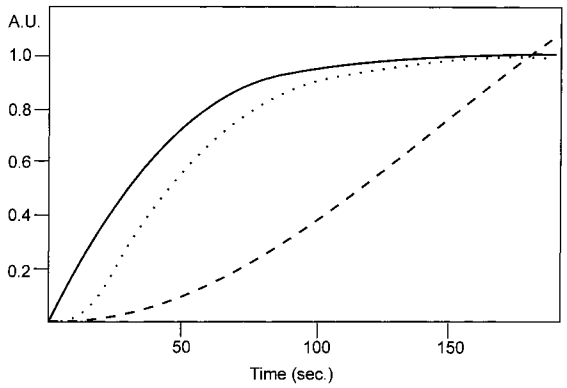

FIGURE 12: Simulation of the time dependence of semiquinone (solid line) and quinone (dashed line) concentration. The time dependence of the velocity of quinone formation in the reaction course is also shown (dotted line). The equations used are eq 23 (solid line), eq 24 (dotted line), and eq 25 (dashed line) described in the Appendix.

$$\frac{1}{V} = \frac{K_m'}{V_{max}'}\frac{1}{[C]} + \frac{1}{V_{max}'} \qquad (27)$$

From the Lineweaver−Burk plots of Figure 6, the K_m' values are 35 mM and 50 mM in the case of *o*-diphenol and methylcatechol, respectively. Since the value of K_m' is related to K_m, one obtains, taking $K_0 = 0.09$ mM and $[O_2] = 0.28$ mM, $K_m = 26.5$ mM and $K_m = 37.8$ mM (for *o*-diphenol and methylcatechol, respectively), in very good agreement with the results of *W* versus substrate concentration (eqs 18 and 20).

REFERENCES

1. van Holde, K. E., and Miller, K. I. (1995) *Adv. Protein Chem. 47*, 1−81.
2. Volbeda, A., and Hol, W. G. J. (1989) *J. Mol. Biol. 209*, 249−279.
3. Hazes, B., Magnus, K., Bonaventura, C., Bonaventura, J., Dauter, Z., Kalk, K. H., and Hol, W. G. J. (1993) *Protein Sci. 2*, 597−619.
4. Magnus, K., and Ton-That, H. (1992) *Chem. Rev. 94*, 727−735.
5. Magnus, K. A., Hazes, B., Ton-That, H., Bonaventura, C., Bonaventura, J., and Hol, W. G. J. (1994) *Proteins: Struct., Funct., Genet. 19*, 302−309.
6. Woolery, G. L., Powers, L., Winkler, M., Solomon, E. I., and Spiro, T. G. (1984) *J. Am. Chem. Soc. 106*, 86−92.
7. Solomon, E. I. (1981) in *Copper Proteins* (Spiro, T. G., Ed.) pp 43−108, J. Wiley, New York.
8. Cuff, M. E., Miller, K. I., van Holde, K. E., and Hendrickson, W. A. (1998) *J. Mol. Biol. 278*, 855−870.
9. Woolery, G. L., Powers, L., Winkler, M., Solomon, E. I., Lerch, K., and Spiro, T. G. (1984) *Biochim. Biophys. Acta 788*, 155−161.
10. Lerch, K. (1981) *Met. Ions Biol. Syst. 13*, 143−186.
11. Wilcox, D. E., Porras, A. G., Hwang, Y. T., Lerch, K., Winkler, M., and Solomon, E. I. (1985) *J. Am. Chem. Soc. 107*, 4015−4027.
12. Kuiper, H. A., Finazzi-Agrò, A., Antonini, E., and Brunori, M. (1980) *Proc. Natl. Acad. Sci. U.S.A. 77*, 2387−2389.
13. Finazzi-Agrò, A., Zolla, L., Flamigni, L., Kuiper, H. A., and Brunori, M. (1982) *Biochemistry 21*, 415−418.
14. Beltramini, M., Salvato, B., Santamaria, M., and Lerch, K. (1990) *Biochim. Biophys. Acta 1040*, 365−372.
15. Beltramini, M., Bubacco, L., Salvato, B., Casella, L., Gullotti, M., and Garofani, S. (1992) *Biochim. Biophys. Acta 1120*, 24−32.

16. Nakahara, A., Suzuki, S., and Kino, J. (1983) *Life Chem. Rep. 1, Suppl. 1*, 319−322.
17. Zlateva, T., Di Muro, P., Salvato, B., and Beltramini, M. (1996) *FEBS Lett. 384*, 251−254.
18. Salvato, B., Ghiretti-Magaldi, A., and Ghiretti, F. (1979) *Biochemistry 18*, 2731−2736.
19. Bubacco, L., Magliozzo, R. S., Beltramini, M., Salvato, B., and Peisach, J. (1992) *Biochemistry 31*, 9294−9303.
20. Salvato, B., Giacometti, G. M., Beltramini, M., Zilio, F., Giacometti, G., Magliozzo, R. S., and Peisach, J. (1989) *Biochemistry 28*, 680−684.
21. Beltramini, M., Bubacco, L., Casella, L., Alzuet, G., Gullotti, M., and Salvato, B. (1995) *Eur. J. Biochem. 232*, 98−105.
22. Beltramini, M., Santamaria, M., and Salvato, B. (1988) *Arch. Biochem. Biophys. 262*, 149−158.
23. Beltramini, M., Santamaria, M., Salvato, B., and Lerch, K. (1990) *Biol. Met. 3*, 93−97.
24. Lerch, K. (1983) *Mol. Cell. Biochem. 52*, 125−130.
25. Klotz, I. M., and Klotz, T. A. (1955) *Science 121*, 477−480.
26. Winkler, M., Lerch, K., and Solomon, E. I. (1981) *J. Am. Chem. Soc. 103*, 7001−7003.
27. Huber, M., and Lerch, K. (1986) in *Invertebrate Oxygen Carriers* (Linzen, B., Ed.) pp 265−276, Springer-Verlag, Berlin.
28. Lerch, K., Huber, M., Schneider, H. J., Drexel, R., and Linzen, B. (1986) *J. Inorg. Biochem. 26*, 213−217.
29. Fujimoto, K., Okino, N., Kawabata, S., Iwanaga, S., and Ohnishi, E. (1995) *Proc. Natl. Acad. Sci. U.S.A. 92*, 7769−7773.
30. Solomon, E. I., Baldwin, M. J., and Lowery, M. D. (1992) *Chem. Rev. 92*, 521−542.
31. Kupper, U., Niedermann, D. M., Travaglini, G., and Lerch, K. (1989) *J. Biol. Chem. 264*, 17250−17258.

BI980879J